Modulation of pairing interaction in $Bi_2Sr_2CaCu_2O_{8+\delta}$ by an O dopant: A density functional theory study

Kateryna Foyevtsova,[1] H. C. Kandpal,[2] Harald O. Jeschke,[1] S. Graser,[3] H.-P. Cheng,[4]
Roser Valentí,[1] and P. J. Hirschfeld[4]

[1]*Institut für Theoretische Physik, Goethe-Universität Frankfurt, 60438 Frankfurt am Main, Germany*
[2]*IFW Dresden, P.O. Box 270016, D-01171 Dresden, Germany*
[3]*Zentrum für Elektronische Korrelationen und Magnetismus, Institut für Physik, Universität Augsburg, 86135 Augsburg, Germany*
[4]*University of Florida, Gainesville, Florida 32611, USA*

Scanning tunneling spectroscopy measurements on the high-temperature superconductor $Bi_2Sr_2CaCu_2O_{8+\delta}$ have reported an enhanced spectral gap in the neighborhood of O dopant atoms. We calculate, within density functional theory (DFT), the change in electronic structure due to such a dopant. We then construct and discuss the validity of several tight-binding (TB) fits to the DFT bands with and without an O dopant. With the doping-modulated TB parameters, we finally evaluate the spin susceptibility and pairing interaction within spin-fluctuation theory. The d-wave pairing eigenvalues are enhanced above the pure system without O dopant, supporting the picture of enhanced local pairing around such a defect.

I. INTRODUCTION

With the observation in scanning tunneling spectroscopy (STS) measurements on high-T_c Bi-based cuprate superconductors[1] that the oxygen dopant position and the size of the superconducting gap are correlated, it has become evident that dopant atoms may influence superconductivity beyond their roles as sources of mobile charge and scattering centers. Subsequently, Nunner *et al.*[2] showed that many STS observations can be explained if one assumes that dopants locally enhance the pairing interaction. It is clearly desirable to further justify the proposal of Ref. 2 by identifying the microscopic mechanism responsible for the local pairing interaction enhancement. Such a step would fulfill a longstanding goal of allowing the systematic study of the pairing interaction itself by the measurement and modeling of the effects which modulate it.

If we accept the dominance of a magnetically driven pairing mechanism in the cuprates, the pairing enhancement is a result of the local increase in the spin-fluctuation exchange interaction in the vicinity of a dopant, which can occur due to the dopant-induced local structural modifications. Whether the structural and the corresponding local electronic-structure modifications can indeed enhance the local superexchange coupling has been a subject of several recent studies.[3–5] The problem is typically treated by calculating the local exchange coupling constants of the t-J model, the large-U limit of the Hubbard model, with the assumption that the local parameters of the latter (the on-site energy μ and the hopping integrals t) are modified due to the presence of a dopant. In Ref. 5, by means of the Rayleigh-Schrödinger perturbation expansion it was shown for the three-band Hubbard model that the exchange coupling is enhanced only in a certain region of the Hubbard model parameters phase diagram. Unfortunately, recent numerical estimates of the parameter values of the Hubbard model with an impurity based on electrostatic calculations[4] place the dopant-induced variation in the region of the phase diagram where exchange gets

suppressed. Though discouraging at first glance, it is clear that this general approach contains many oversimplifications of the true electronic structure. In addition, the full pairing interaction, while related to the exchange coupling J, can be influenced also by dynamical spin-fluctuation processes.[6] We have therefore been stimulated to investigate further the dopant-induced effects on the local pairing with the goal of improving the model by a refinement of the approximations. For instance, besides considering the variation in the atomic on-site energies (which was assumed in Refs. 3 and 5 to be the only effect due to a dopant) one can allow for the variation in hopping integrals near the dopant as well. One can furthermore go beyond the electrostatic considerations in calculating the inhomogeneous Hubbard model parameters in order to place more accurately the exchange coupling variations in the parameter phase diagram by employing *ab initio* calculations. Finally, one can directly calculate the dynamical pairing interaction within weak coupling spin-fluctuation theory. These are the aims of the present work.

In this paper, we perform density functional theory (DFT) calculations for $Bi_2Sr_2CaCu_2O_{8+\delta}$ and explore the possibility of extracting out of the electronic-structure reliable effective Cu-Cu hopping integrals t and on-site energies μ as a function of oxygen doping. In general, DFT calculations of the electronic structure near the Fermi surface of cuprate materials are not considered reliable due to strong correlation effects but it has been argued that *changes* in electronic structure induced by high-energy impurity states are much less sensitive. These effective parameters are further considered in the Hubbard model calculations of the spin susceptibility and superconducting gap function, and key changes in these functions are observed which support the importance of the effect of the oxygen dopants on the pair correlations in these materials.

The evaluation of the hopping integrals and on-site energies of the Hubbard model is performed by mapping the eigenvalues of the corresponding noninteracting tight-binding (TB) Hamiltonian to the valence bands of
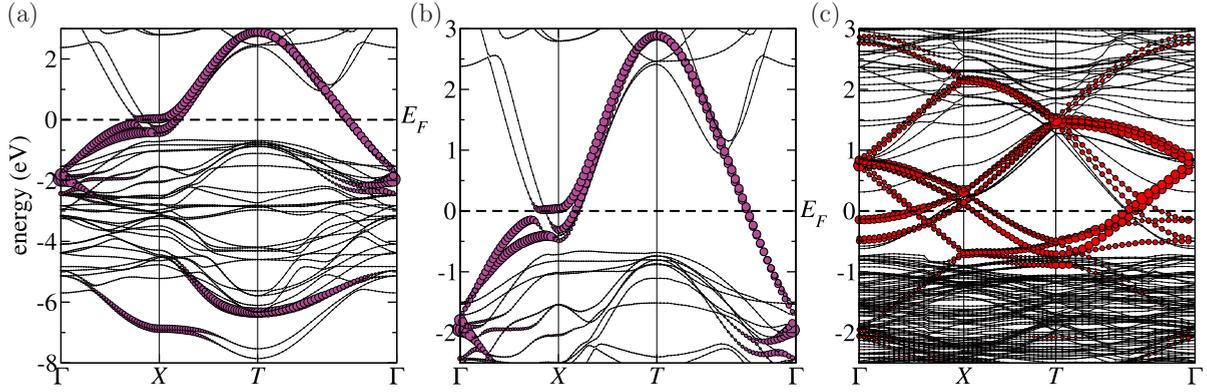
FIG. 1. (Color online) [(a) and (b)] DFT electronic band structure of $Bi_2Sr_2CaCu_2O_8$ shown for different energy ranges. (c) Band structure of the O-doped $Bi_2Sr_2CaCu_2O_{8+\delta}$ supercell in the same energy window as (b). The weight of the Cu $3d_{x^2-y^2}$ character in the eigenvalues is proportional to the circles' size.

$Bi_2Sr_2CaCu_2O_{8+\delta}$ as a function of oxygen doping. Although $Bi_2Sr_2CaCu_2O_{8+\delta}$ is more accurately described by the three-band model,[5] here we consider a single-band TB Hamiltonian, with the single active orbital being the Cu $3d_{x^2-y^2}$ orbital at the Fermi level as the simplest case for the proposed approach. In fact, recent studies showed that the one-band Hubbard model suffices to describe the important features of the low-energy physics in the cuprates.[7] We find that the accuracy of the dopant-induced TB Hamiltonian parametrization suffers from two sources of uncertainty, which are (i) the presence of effective far Cu neighbor interactions in the homogeneous model (undoped case) allowing for many alternative parameter sets and (ii) the need to reduce the enormous number of adjustable parameters of the dopant-induced TB model in order to perform the numerical optimization. In view of these considerations we present two alternative TB models and discuss their validity in terms of physical arguments.

II. ELECTRONIC-STRUCTURE CALCULATIONS

The electronic-structure calculations for the parent compound $Bi_2Sr_2CaCu_2O_8$ were performed with the reference crystal structure reported in Ref. 8. $Bi_2Sr_2CaCu_2O_8$ crystallizes in the space group $I4/mmm$, with a unit cell which we consider in the tetragonal symmetry (see Ref. 9 for the discussion on the structural supermodulation in $Bi_2Sr_2CaCu_2O_8$), consisting of two identical slabs of atoms, one shifted with respect to the other by a vector $(a/2, a/2, c/2)$, where a and c are the lattice parameters of a tetragonal unit cell. Oxygen doping of this system was modeled by introducing one extra interstitial oxygen atom into a surface supercell consisting of eight primitive unit cells in the xy plane. We consider the surface supercell in order to reproduce the conditions of a typical STM experiment on an O-doped $Bi_2Sr_2CaCu_2O_{8+\delta}$ surface. The electronic-structure calculations in the present work were performed with the linearized-augmented-plane-wave basis, as implemented in WIEN2K.[10] The exchange and correlation effects were treated within the generalized gradient approximation as implemented by Perdew, Burke, and Ernzerhof.[11] Additional de-

tails of the electronic structure calculations are given in Appendix A

In Fig. 1(a) we present the electronic band structure of $Bi_2Sr_2CaCu_2O_8$ in the energy window between $[-8 \text{ eV}, 3 \text{ eV}]$. The two Cu $3d_{x^2-y^2}$ bands of the parent compound are marked by circles with sizes proportional to the $3d_{x^2-y^2}$ weight. They are rather dispersive, which is a typical feature of the cuprate family.[12] The two Cu bands crossing the Fermi level are the antibonding bands in the chemical bonding between Cu atoms and the O atoms in the superconducting layer. The bonding bands lie in the region between $[-8 \text{ eV}, -5 \text{ eV}]$. In the following we concentrate on the energy window $[-2.5 \text{ eV}, 3 \text{ eV}]$ near the Fermi level E_F as indicated in Fig. 1(b). At the $X = (\pi, 0, 0)$ point the Cu $3d_{x^2-y^2}$ bands show a strong overlap with the Bi-O bands near the Fermi level, and at the $\Gamma = (0, 0, 0)$ point there is strong hybridization between the Cu $3d_{x^2-y^2}$ and some of the lower lying O $2p$ and Cu $3d$ bands.

Figure 1(c) presents the band structure of the O-doped $Bi_2Sr_2CaCu_2O_{8+\delta}$ supercell in the same energy range. The band structure of the supercell is plotted along the same high symmetry points in the Brillouin zone as those of the parent compound. However, since the doped systems' unit cell is eight times larger than the parent compound unit cell, its Brillouin zone shrinks and the bands fold on top of each other so that effectively there are 16 Cu $3d_{x^2-y^2}$ bands crossing the Fermi level, where 16 is the number of Cu atoms in the supercell slab.

Because the Brillouin zones of the parent compound and of the doped supercell are defined differently, it is not straightforward to compare their band structures. In order to make such a comparison, we recalculate the electronic structure of the parent compound in the folded Brillouin zone. Once this is done, small but traceable changes in the shape of the Cu $3d_{x^2-y^2}$ bands as a function of oxygen doping become apparent as will be shown in the next sections. We will dedicate the rest of the paper to the quantitative evaluation of these changes in terms of hopping integrals of a single-band tight-binding Hamiltonian as well as calculations of the spin susceptibility and superconducting pairing function.

TABLE I. TB1$_{undoped}$ results: optimized values of the on-site energy μ and the hopping integrals $t_{\mathbf{l}}$ between 12 Cu nearest neighbors in eV. These parameters reproduce the Cu $3d_{x^2-y^2}$ bands in Figs. 2(a) and 2(b). The vector $\mathbf{l}=(n,m,z)$ is given by integers n,m; z can take values of 0 or $z=0.099$ as $0.099c$ is the distance between two CuO$_2$ layers.

μ	t_{00z}	t_{100}	t_{10z}	t_{110}	t_{11z}	
0.4212	0.0543	-0.5196	0.0056	0.1115	-0.0221	
t_{200}	t_{20z}	t_{210}	t_{21z}	t_{220}	t_{22z}	t_{300}
-0.0859	0.0117	-0.0078	-0.0064	0.0025	-0.0103	-0.0238

III. SINGLE-BAND TIGHT-BINDING MODEL

A. Parent compound

A standard procedure to analyze the low-energy band structure features of solid state systems is the TB parametrization.[13,14] Since the symmetry of the parent compound Bi$_2$Sr$_2$CaCu$_2$O$_8$ unit cell is $I4/mmm$ and the number of distinct hopping integrals (adjustable parameters) is small, the TB parametrization in this case is straightforward and has been already performed in previous studies.[12,15] The complexity of the problem is dramatically increased when trying to obtain the TB parameters for the doped supercell bands shown in Fig. 1(c): first, because the number of bands to be mapped increases by a factor of 8, which means that, in order to optimize the TB parameters, a global minimum of a complex mathematical function expressed by a 16×16 matrix needs to be found; second, because the number of distinct hopping integrals is expected to rise considerably as we increase the size of the unit cell and lower its symmetry. Our strategy to overcome these complications is to use the hopping integrals obtained for the parent compound Cu $3d_{x^2-y^2}$ bands as starting values for parametrizing the doped supercell bands.

An important point to consider is that the differences between the Cu $3d_{x^2-y^2}$ bands of the parent and doped compounds are small, which is reasonable since we do not expect the interstitial oxygen to have a drastic effect on the orbital overlap of its neighboring Cu atoms. Therefore, the TB parameters for the Cu $3d_{x^2-y^2}$ bands in the parent and doped compounds must be obtained with a fitting error smaller than the dopant-induced differences in the band structure, i.e., the quality of both TB mappings must be particularly high. For this reason we consider the antibonding Cu $3d_{x^2-y^2}$ bands over the entire energy range over which they disperse. We find that, in order to *accurately* reproduce the DFT Cu $3d_{x^2-y^2}$ bands of the parent compound [Fig. 1(a)], up to 13 Cu-Cu neighbors have to be included in the model TB Hamiltonian. We should note, however, that among these various hopping integrals, those representing hybridizations between the far neighbors are only effective parameters; we are forced to include them in the single-band model in order to describe those features of the Cu $3d_{x^2-y^2}$ bands that stem from the interaction of the Cu $3d_{x^2-y^2}$ orbital with other Cu $3d$ orbitals and the O $2p$ orbitals. For example, near $\Gamma = (0,0,0)$ the Cu $3d_{x^2-y^2}$ bands are anomalously flat and show an $\epsilon_k \propto k^4$ behavior,[15] where k is the momentum in the Brillouin zone. In order to reproduce this feature, inclusion of higher harmonics is required in the model equations.

The long range effective hoppings which arise from the mapping of the complex band structure over a $\sim$5 eV range onto a single band model are found to be much smaller than the short range hoppings, e.g., t_{100} and t_{110}. This strongly suggests that it will be difficult to identify a unique param-

TABLE II. TB2$_{undoped}$ results: optimized values of the on-site energy μ and hopping integrals $t_{\mathbf{l}}$ for the parent compound where only the closest nearest neighbors are considered. Also shown are the TB results obtained by mapping the doped supercell bands to a homogeneous Hamiltonian (TB2$_{hom.\ doped}$). The meaning of the three subindices is the same as in Table I.

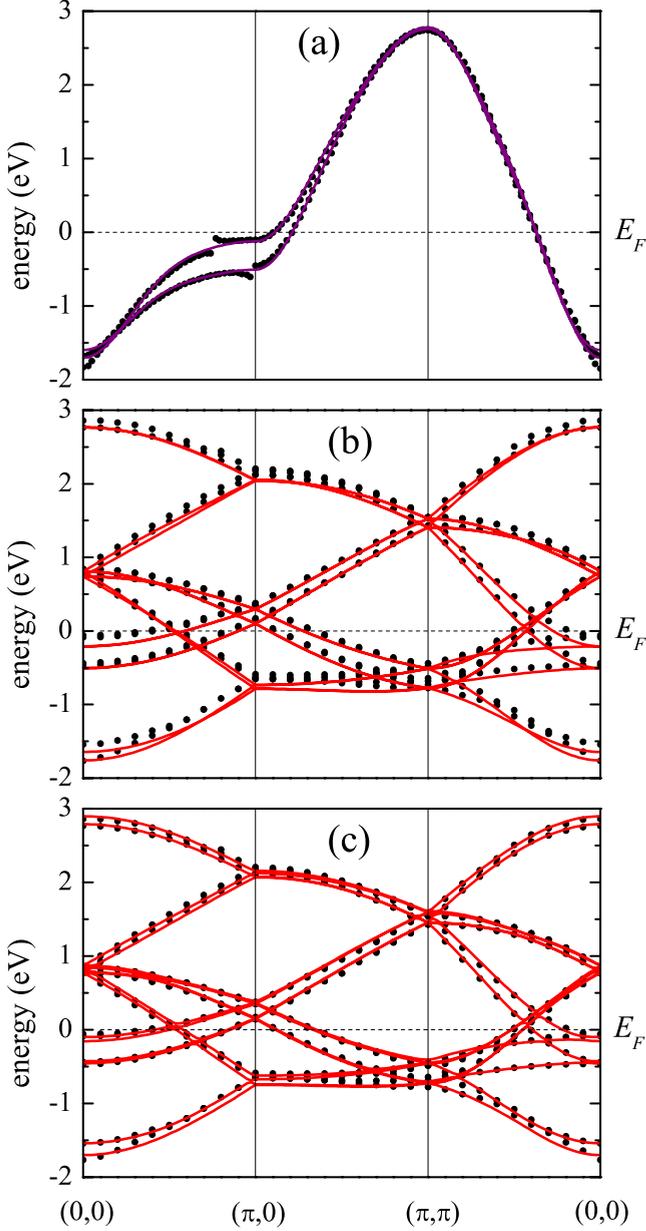|	μ	t_{100}	t_{110}	t_{200}	t_{00z}
TB2$_{undoped}$	0.4464	-0.5174	0.1085	-0.0805	0.0818
TB2$_{hom.\ doped}$	0.4900	-0.5150	0.1158	-0.0800	0.0700
	t_{11z}	t_{210}	t_{300}	t_{400}	t_{21z}
TB2$_{undoped}$	-0.0264	-0.0073	-0.0182	-0.0122	-0.0044
TB2$_{hom.\ doped}$	-0.0229	-0.0075	-0.0177	-0.0046	-0.0062
	t_{220}	t_{330}	t_{500}	t_{33z}	
TB2$_{undoped}$	0.0068	-0.0052	-0.0049	-0.0047	
TB2$_{hom.\ doped}$	0.0045	-0.0015	-0.0012	-0.0003	

FIG. 2. (Color online) Plot of the DFT calculated Cu $3d_{x^2-y^2}$ bands (dots) and the TB1 Hamiltonian spectrum (lines) for $Bi_2Sr_2CaCu_2O_8$ and $Bi_2Sr_2CaCu_2O_{8+\delta}$: (a) comparison of the $Bi_2Sr_2CaCu_2O_8$ electronic structure to the TB1$_{undoped}$ model; (b) comparison of the $Bi_2Sr_2CaCu_2O_{8+\delta}$ electronic structure to the TB1$_{undoped}$ model plotted in the folded Brillouin zone; and (c) comparison of the $Bi_2Sr_2CaCu_2O_{8+\delta}$ electronic structure to the TB1$_{loc.\ doped}$ model (see Fig. 4). High symmetry points are given by (k_x, k_y) only, $k_z = 0$; thus $(0,0) = \Gamma$, $(\pi, 0) = X$, and $(\pi, \pi) = T$.

eter set. Alternative single-band models can exist corresponding to different choices of effective hopping paths. We therefore discuss two possible sets of single-band TB Hamiltonian parameters (presented in Tables I and II) to give a sense of how robust the TB models can be. Details of the construction of these models are found in the Appendix B. Both sets are indeed found to describe the Cu $3d_{x^2-y^2}$ bands in the parent compound equally well. In the following we will adopt the notation: (1) TB1: 12 hopping parameters, six
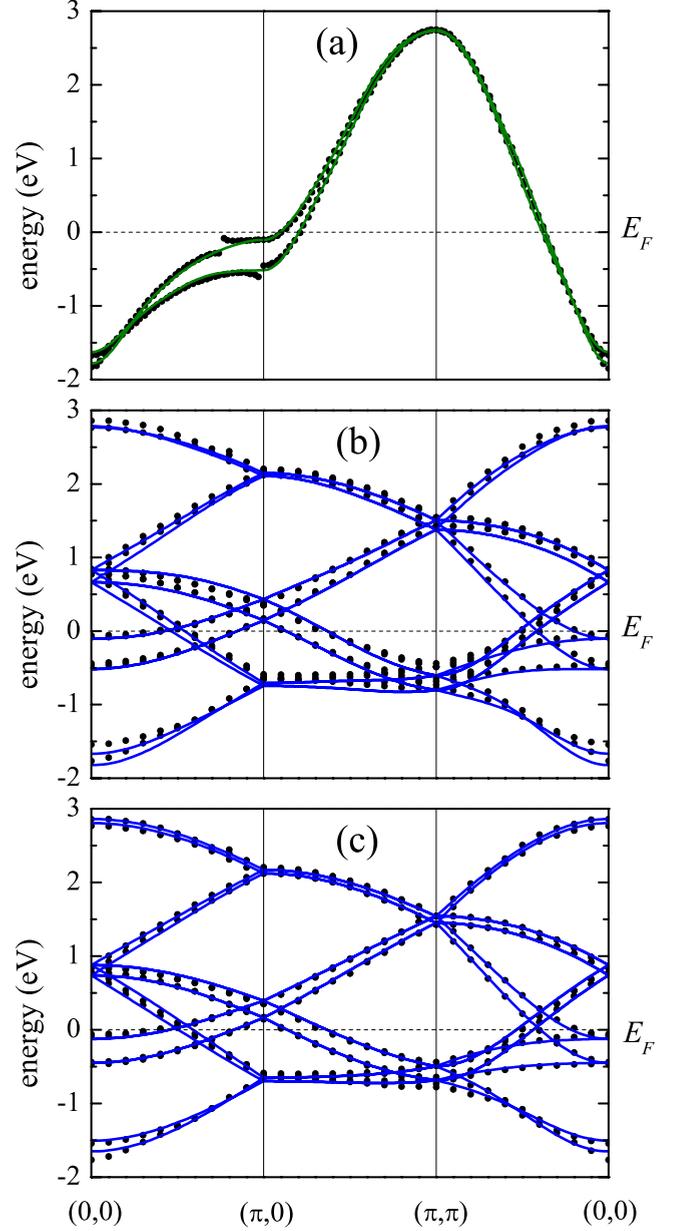
FIG. 3. (Color online) Plot of DFT calculated Cu $3d_{x^2-y^2}$ bands (dots) and the TB2 Hamiltonian spectrum (line) for $Bi_2Sr_2CaCu_2O_8$ and $Bi_2Sr_2CaCu_2O_{8+\delta}$: (a) comparison of the $Bi_2Sr_2CaCu_2O_8$ electronic structure to the TB2$_{undoped}$ model; (b) comparison of the $Bi_2Sr_2CaCu_2O_{8+\delta}$ electronic structure to the TB2$_{undoped}$ model plotted in the folded Brillouin zone; and (c) comparison of the $Bi_2Sr_2CaCu_2O_{8+\delta}$ electronic structure to the homogeneous TB2$_{hom.\ doped}$ model. (Table II second row).

effective interlayer hoppings; (a) TB1$_{undoped}$: undoped parent compound; (b) TB1$_{loc.\ doped}$: TB parameters are taken to vary in the vicinity of O dopant; (2) TB2: 13 hopping parameters, four effective interlayer hoppings; (a) TB2$_{undoped}$: undoped parent compound; (b) TB2$_{hom.\ doped}$: fit is obtained with homogeneous TB parameters over the entire supercell. A discussion of the tight-binding parameters describing the O-doped system will be the subject of the next section.

In Fig. 2(a) the TB1$_{undoped}$ Hamiltonian spectrum in the full Brillouin zone is compared to the DFT bands of the

parent compound. In Fig. 2(b), the spectrum of the TB1$_{undoped}$ Hamiltonian is replotted in the folded Brillouin zone and compared with the Cu $3d_{x^2-y^2}$ bands of the doped supercell. The slight differences between the shapes of the doped supercell DFT bands and of the TB bands of the parent compound are due to the presence of the interstitial oxygen, which displaces the neighboring Cu atoms and thus modifies their corresponding overlap integrals. It is possible to quantify these effects by fine tuning the parameters of the TB Hamiltonian such that the supercell bands are reproduced, as we will show below.

In Fig. 3(a), we now show the corresponding TB2$_{undoped}$ Hamiltonian spectrum in the full Brillouin zone in comparison to the DFT bands of the parent compound. In Fig. 3(b), the same TB bands are plotted in the folded Brillouin zone, together with the DFT bands of the doped supercell. Comparing the TB1$_{undoped}$ and TB2$_{undoped}$ model parameters for the parent compound (Tables I and II), we observe that the TB2$_{undoped}$ model has several features that can be considered an advantage in terms of the physics that the model implies; this model includes only four hopping integrals between the CuO$_2$ layers, t_{00z}, t_{11z}, t_{21z}, and t_{33z}, whose relevance can be justified either by the close proximity of the two Cu atoms (t_{00z}) or by the presence of a Ca atom along the Cu-Cu connection mediating electron hopping (t_{11z}, t_{21z}, and t_{33z}). In the TB1$_{undoped}$ model, on the other hand, the mechanism of some of its six interlayer interactions is not as clear. Furthermore, one would rather expect the contribution of interacting far Cu neighbors within a CuO$_2$ layer to be more important as considered in the TB2$_{undoped}$ model.

In the next section, we will discuss the results of the derivation of the TB Hamiltonian for the O-doped Bi$_2$Sr$_2$CaCu$_2$O$_{8+\delta}$ supercell, obtained when either the parameter set in TB1$_{undoped}$ (Table I) or TB2$_{undoped}$ (Table II) are used as initial values for mapping the supercell DFT bands.

B. O-doped supercell

In order to describe the DFT Cu $3d_{x^2-y^2}$ bands of the doped supercell [Fig. 1(c)] within a TB model, one has to construct a Hamiltonian similar to Eq. (B1), which will be now represented by a 16×16 matrix, according to the number of Cu atoms in the supercell (eight atoms in each CuO$_2$ layer). Since the presence of the interstitial oxygen introduces inhomogeneities in the system, the number of distinct model parameters for the supercell is not defined by simply the number of parameters of the corresponding parent unit cell (which is 12 and 13 for the models of Tables I and II, respectively, plus the on-site energy μ), but increases considerably. For instance, even by taking into account the mirror plane symmetry, there are still 238 parameters in the supercell TB Hamiltonian based on the TB1$_{undoped}$ *ansatz*. Technically, it is impossible to find a unique and unambiguous set of parameters by performing an optimization of such a huge number of parameters, especially since our aim is to capture the slight differences between the bands of the parent compound and the doped compound [see Figs. 2(b) and 3(b)]. One way to proceed would be to approximate the hopping integrals that become distinct in the supercell due to the in-
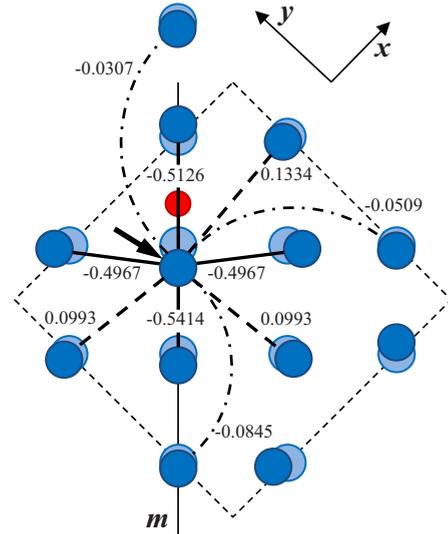

FIG. 4. (Color online) The schematic lattice of dopant-displaced Cu atoms in the oxygen-doped supercell of Bi$_2$Sr$_2$CaCu$_2$O$_{8+\delta}$. The smallest circle represents the interstitial oxygen atom and the larger circles stand for Cu atoms. Darker color is used for Cu atoms in the CuO$_2$ layer closest to the interstitial oxygen. The Cu-Cu bonds that correspond to the hopping integrals of the t_{100} type are represented by solid lines, the hopping integrals of the t_{110} type by dashed lines, and the hopping integrals of the t_{200} type by dash-dotted lines. The numbers over the bonds stand for the optimized values of corresponding hopping integrals of the doped supercell TB model based upon the nearest-neighbors parent compound model (see text). The optimized value of the on-site energy of this model for the Cu in the next-nearest CuO$_2$ layer (the light Cu atom symbols) is μ =0.4445 eV. The six optimized on-site energy values for Cu in the nearest CuO$_2$ layer (the dark Cu atom symbols) are μ=0.5757, 0.5057, 0.5341, 0.5151, 0.4930, and 0.5186 eV. μ=0.5757 eV corresponds to the Cu atom which is displaced most by the dopant and is marked with an arrow. m labels the mirror plane.

homogeneity introduced by the dopant by their average values. In this "averaged" homogeneous TB model for the supercell, there would be as many parameters as in the corresponding model for the parent compound and their optimization would be simple; an example is given in Table II (TB2$_{hom.\ doped}$ row). With such an approach, however, the most interesting physics concerning *local* effects due to the dopant is left out.

The exact knowledge of how the Cu on-site energies and the most relevant Cu-Cu hopping integrals t_{100} and t_{110} are modified near the dopant is very important for understanding the dopant-induced effects on the local spin superexchange coupling,[16–18] which is related to the size of the local superconducting gap in cuprates.[5] Therefore, in order to be able to study the local variations in the model parameters, we propose the following approximate treatment of the problem. We assume that the on-site energies and hopping integrals most affected by the dopant are those that are nearest to the dopant, and we concentrate on the largest TB model parameters, such as μ, t_{100}, and t_{110}. Then, the supercell TB Hamiltonian is optimized by adjusting the selected parameters, while for the rest, i.e., the effective far Cu neighbor interactions, their initial values are preserved. An illustration of the

procedure in the case of the TB1$_\text{undoped}$ model is shown in Fig. 4 and is worked out in detail in Appendix C. It turns out that this approach gives sensible results when the TB super-cell model is built upon the TB1$_\text{undoped}$ model (Table I) and gives counterintuitive results when the TB2$_\text{undoped}$ model for the parent compound (Table II) is used. In Fig. 2(c) we show the good agreement between the energy spectrum of this TB1$_\text{loc. doped}$ Hamiltonian with the DFT bands of Bi$_2$Sr$_2$CaCu$_2$O$_{8+\delta}$.

To conclude this section, we present the *homogeneous* TB model for the doped supercell TB2$_\text{hom. doped}$ based on the TB2$_\text{undoped}$ model [see Table II and Fig. 3(c)]. Even though the homogeneous model does not reflect the local dopant-induced effects, it can still be useful as it provides the information on how the model parameters change on average. For instance, it is interesting to observe that the average ratio t_{110}/t_{100} increases in the doped supercell compared to that in the parent compound (from 0.2097 to 0.2249); this might suggest a possible increase in the superconducting transition temperature upon doping, in analogy with the observation within the cuprate family, that the materials characterized by a larger t_{110}/t_{100} ratio have higher transition temperatures.[19] Unlike the situation with the mapping approach previously discussed, which aimed at capturing local physics, the parameters of the homogeneous Hamiltonian demonstrate the same behavior upon doping regardless of the parent compound TB model (TB1$_\text{undoped}$ and TB2$_\text{undoped}$) chosen as a starting point for mapping the doped supercell electronic structure.

IV. SPIN FLUCTUATION PAIRING

A. Spin susceptibility

In the following we calculate the magnetic spin susceptibilities for the TB models obtained previously, namely, (i) the TB1$_\text{undoped}$ (Table I), (ii) the TB2$_\text{undoped}$ (Table II first row), (iii) the inhomogeneous doped supercell model TB1$_\text{loc. doped}$ (Fig. 4), and (iv) the homogeneous doped super-cell model TB2$_\text{hom. doped}$ (Table II second row). The spin susceptibility is derived within the Matsubara Green's functions formalism[20] from the noninteracting Green's functions. In a general formulation, the spin susceptibility is a function of four orbital indices, $(\chi_s)_{st}^{pq}$, which, in the considered case of a single orbital but multiple atoms in a unit cell, refer to the orbitals on different atoms. For the noninteracting case, the spin susceptibility $(\chi_s)_{st}^{pq}$ is equivalent to the charge suscep-tibility $(\chi_c)_{st}^{pq}$, $(\chi_s)_{st}^{pq}=(\chi_c)_{st}^{pq}\equiv\chi_{st}^{pq}$, and is given by[14]

$$\chi_{st}^{pq}(\mathbf{q},\omega) = -\frac{1}{N_kN}\sum_{\mathbf{k},\mu\nu}\{f[E_\nu(\mathbf{k}+\mathbf{q})] - f[E_\mu(\mathbf{k})]\}$$

$$\times \frac{a_\mu^s(\mathbf{k})a_\mu^{p*}(\mathbf{k})a_\nu^q(\mathbf{k}+\mathbf{q})a_\nu^{t*}(\mathbf{k}+\mathbf{q})}{\omega + E_\nu(\mathbf{k}+\mathbf{q}) - E_\mu(\mathbf{k}) + i0^+}. \quad (1)$$

In this expression, indices s, p, q, and t refer to the N Cu atoms in the unit cell and run from 1 to N while indices μ and ν distinguish the N eigenvalues $E(\mathbf{k})$ of the diagonalized TB Hamiltonian. The matrix elements $a_\mu^s(\mathbf{k})$ are the components of the eigenvectors of the TB Hamiltonian. The inte-
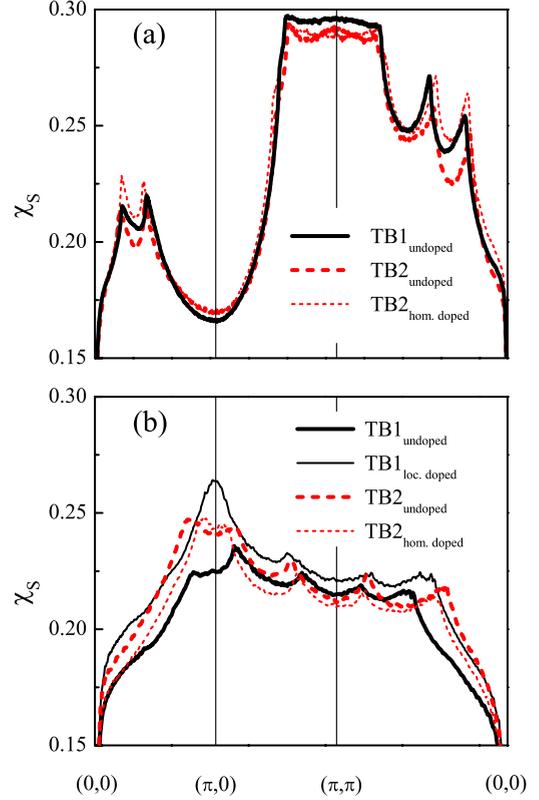

FIG. 5. (Color online) The static spin susceptibility of (a) the two parent compound TB models TB1$_\text{undoped}$ and TB2$_\text{undoped}$ and the homogeneous doped supercell model TB2$_\text{hom. doped}$, plotted in the full Brillouin zone, and (b) the two parent compound TB models TB1$_\text{undoped}$ and TB2$_\text{undoped}$ and the inhomogeneous TB1$_\text{loc. doped}$ and homogeneous TB2$_\text{hom. doped}$ doped supercell models, plotted in the folded Brillouin zone.

gration over the Brillouin zone has been replaced by a sum over a sufficiently large number $N_\mathbf{k}$ of k points. $f(E)$ is the Fermi-Dirac distribution function. In the following, we will focus on the static noninteracting spin susceptibility $\chi_S(\mathbf{q})$

$$\chi_S(\mathbf{q}) = \frac{1}{2}\sum_{sp}\chi_{ss}^{pp}(\mathbf{q},\omega=0) \quad (2)$$

and examine its behavior in the four cases of interest along the main symmetry directions in the Brillouin zone.

The static spin susceptibilities $\chi_S(\mathbf{q})$ of the parent com-pound calculated with the TB1$_\text{undoped}$ model of Table I (bold black line) and with the TB2$_\text{undoped}$ model of Table II (bold dashed line) are plotted in Fig. 5(a). The two susceptibilities show similar features with double peaks along $(0,0,0)$ $-(\pi,0,0)$ and $(\pi,\pi,0)-(0,0,0)$ directions and a broad pla-teau at $(\pi,\pi,0)$. These similarities can be understood in terms of the fact that most important parameters in the two TB models (t_{100}, t_{110}, etc.) have close values. In this respect, it is not surprising that the spin susceptibility calculated with the averaged TB parameters of the homogeneous Hamil-tonian TB2$_\text{hom. doped}$ for Bi$_2$Sr$_2$CaCu$_2$O$_{8+\delta}$ [thin dashed line in Fig. 5(a)] qualitatively reproduces the same behavior as the TB models for the parent compound.

We next calculate the spin susceptibility with the *inhomogeneous* TB Hamiltonian for the doped Bi$_2$Sr$_2$CaCu$_2$O$_{8+\delta}$ supercell TB1$_{loc.\ doped}$. Of course in this case the spin susceptibility must be calculated with the full supercell (16×16) Hamiltonian matrix and accordingly is defined in the folded Brillouin zone. Figure 5(b) shows the spin susceptibility calculated with the inhomogeneous TB1$_{loc.\ doped}$ model (thin black line) and, for comparison, the two parent compound susceptibilities replotted in the folded Brillouin zone [as in Fig. 5(a), bold black and bold dashed lines]. Within the inhomogeneous model, a pronounced peak in the spin susceptibility evolves at $(\pi,0,0)$ upon doping whereas in both parent compound susceptibilities this region is featured by a shallow minimum in between two asymmetrical peaks located at some distance from $(\pi,0,0)$. A peak in the spin susceptibility of a noninteracting system can transform into a divergence indicating magnetic instabilities and possible ordering, when the interparticle interactions are switched on. $(\pi,0,0)$ corresponds to a commensurate antiferromagnetic striped order with period $2\sqrt{2}a$ with stripes along the (110) direction of the parent compound unit cell.

B. Superconducting gap function

We consider now the models TB1$_{undoped}$ and TB1$_{loc.\ doped}$ in order to analyze the superconducting properties of the undoped and doped Bi$_2$Sr$_2$CaCu$_2$O$_{8+\delta}$, respectively. We calculate the pairing vertex by assuming that superconductivity in the high-T_c cuprates is driven by the exchange of spin and charge fluctuations.[21] The many-body effects of the Coulomb interaction are here treated within the random phase approximation (RPA).

In order to calculate the pairing vertex, the RPA charge and spin susceptibilities, $\chi_c^{RPA}(\mathbf{q},\omega)$ and $\chi_s^{RPA}(\mathbf{q},\omega)$, are required. They can be obtained from the noninteracting susceptibility $\chi(\mathbf{q},\omega)$ in the form of Dyson-type equations as

$$(\chi_c^{RPA})_{st}^{pq} = \chi_{st}^{pq} - \sum_{uvwz} (\chi_c^{RPA})_{uv}^{pq}(U^c)_{wz}^{uv}\chi_{st}^{wz} \qquad (3)$$

and

$$(\chi_s^{RPA})_{st}^{pq} = \chi_{st}^{pq} + \sum_{uvwz} (\chi_s^{RPA})_{uv}^{pq}(U^c)_{wz}^{uv}\chi_{st}^{wz}. \qquad (4)$$

For a single-band model, only the diagonal U^c and U^s matrices' components are nonzero

$$(U^c)_{ii}^{ii} = U, \quad (U^s)_{ii}^{ii} = U, \qquad (5)$$

where U is the strength of the on-site intraband Coulomb repulsion between electrons. The singlet pairing vertex is then given by

$$\Gamma_{st}^{pq}(\mathbf{k},\mathbf{k}',\omega) = \left[\frac{3}{2}U^s\chi_s^{RPA}(\mathbf{k}-\mathbf{k}',\omega)U^s + \frac{1}{2}U^s \right.$$
$$\left. - \frac{1}{2}U^c\chi_c^{RPA}(\mathbf{k}-\mathbf{k}',\omega)U^c + \frac{1}{2}U^c \right]_{ps}^{tq}. \qquad (6)$$

The scattering of a Cooper pair from the state $(\mathbf{k},-\mathbf{k})$ to the state $(\mathbf{k}',-\mathbf{k}')$ on the Fermi surface is determined by the projected interaction vertex
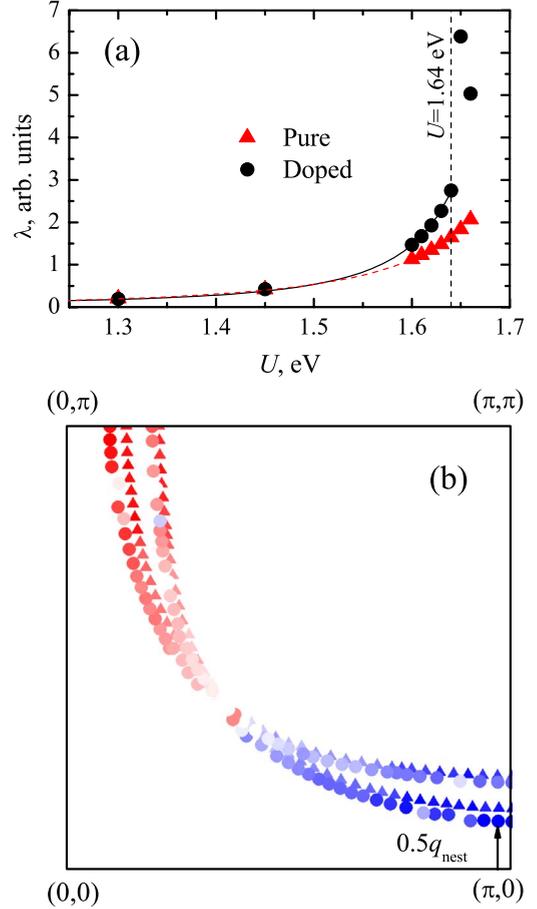

FIG. 6. (Color online) (a) The pairing strength λ for the undoped (triangles) and doped (circles) Bi$_2$Sr$_2$CaCu$_2$O$_{8+\delta}$ TB models as a function of Coulomb repulsion U. (b) The superconducting gap function $g(\mathbf{k})$ on the k-point mesh at the Fermi surface of the undoped Bi$_2$Sr$_2$CaCu$_2$O$_8$ unit cell for the undoped (triangles) and doped (circles) models. Positive $g(\mathbf{k})$ values are mostly above the $(0,0)-(\pi,\pi)$ line (red), negative values mostly below (blue). The intensity of the color is proportional to the absolute value of $g(\mathbf{k})$. Half the nesting vector q_{nest} is shown by an arrow.

$$\Gamma(\mathbf{k},\mathbf{k}',\omega) = \sum_{stpq} a_\nu^t(-\mathbf{k})a_\nu^s(\mathbf{k})\Gamma_{st}^{pq}(\mathbf{k},\mathbf{k}',\omega)a_{\nu'}^{p,*}(\mathbf{k}')$$
$$\times a_{\nu'}^{q,*}(-\mathbf{k}'), \qquad (7)$$

where indices ν and ν' refer to the eigenvectors of the TB Hamiltonian with the corresponding energy eigenvalues close to the Fermi level. As the strength of the pairing interaction is defined by a frequency integral of the imaginary part of $\Gamma(\mathbf{k},\mathbf{k}',\omega)$ weighted by ω^{-1}, it is sufficient to consider the real part of $\Gamma(\mathbf{k},\mathbf{k}',\omega=0)$ according to the Kramers-Kronig relation

$$\int_0^\infty d\omega \frac{\text{Im}[\Gamma(\mathbf{k},\mathbf{k}',\omega)]}{\pi\omega} = \text{Re}[\Gamma(\mathbf{k},\mathbf{k}',\omega=0)]. \qquad (8)$$

If the superconducting gap is decomposed into an amplitude Δ and a normalized gap function $g(\mathbf{k})$, the latter can be evaluated from the following eigenvalue equation:

$$-\oint \frac{d\mathbf{k}'_\parallel}{2\pi} \frac{1}{2\pi v_F(\mathbf{k}')} \Gamma^{\mathrm{symm}}(\mathbf{k},\mathbf{k}') g(\mathbf{k}') = \lambda g(\mathbf{k}). \qquad (9)$$

Here

$$\Gamma^{\mathrm{symm}}(\mathbf{k},\mathbf{k}') = \frac{1}{2} \mathrm{Re}[\Gamma(\mathbf{k},\mathbf{k}',0) + \Gamma(\mathbf{k},-\mathbf{k}',0)] \qquad (10)$$

is the symmetric part of the full interaction and

$$v_F(\mathbf{k}) = |\nabla_\mathbf{k} E_\nu(\mathbf{k})| \qquad (11)$$

is the Fermi velocity at point $\mathbf{k}$ on the Fermi surface. The largest eigenvalue λ of Eq. (9) determines the superconducting transition temperature and its corresponding eigenfunction $g(\mathbf{k})$ has the symmetry of the gap.

We have solved the eigenvalue problem (9) for the undoped and doped $\mathrm{Bi_2Sr_2CaCu_2O_{8+\delta}}$ models in the folded Brillouin zone of the supercell. The folded Brillouin zone has been considered in both cases in order to ensure that the eigenvalue equations are constructed under the same conditions, which is important when the resulting pairing strengths are compared. The calculations have been performed for the temperature $T=0.01$ eV and we considered Coulomb repulsion U values that range from 1.00 to 1.66 eV. Note that these values represent renormalized values of the Hubbard U appropriate for RPA treatments and are smaller than bare U's.[22]

We find that the doped $\mathrm{Bi_2Sr_2CaCu_2O_{8+\delta}}$ model is characterized by a larger value of the pairing strength λ compared to that of the undoped model. The pairing strengths for the two models are presented in Fig. 6(a) as a function of U. Below $U \sim 1.5$ eV the two λ values are almost equal but at larger U values the pairing strength for the doped model grows faster and diverges at $U=1.65$ eV.

Figure 6(b) displays the gap functions $g(\mathbf{k})$ of the undoped and doped models, corresponding to the leading eigenproblem solutions λ of Fig. 6(a) at $U=1.64$ eV. The result from Eq. (9) $g(\mathbf{k})$ is defined on the mesh of k points at the Fermi surface of the folded Brillouin zone. In Fig. 6(b), the k-point mesh was unfolded to the Brillouin zone of the undoped compound unit cell in order to allow a comparison of the Fermi surface behavior for the two systems with experiment. One should note that in the case of the doped supercell such an unfolding is, strictly speaking, not allowed and results in a tearing of the Fermi surface. Yet, since the symmetry lowering effects caused by a dopant are small, the unfolding in this case is a reasonable approximation. In particular, the unfolded way of presenting $g(\mathbf{k})$ allows us to observe that the symmetry of the undoped model $g(\mathbf{k})$ is $d_{x^2-y^2}$ and that upon doping it is roughly preserved, though slightly distorted. We also note the characteristic reduction of the norm of the nesting wave vector q_{nest}, associated with the occurrence of the spin density wave state, in the doped case. This behavior is in agreement with ARPES results for $\mathrm{Bi_2Sr_2CaCu_2O_{8+\delta}}$.[23]

The gap equation calculations presented here show that the TB model derived for the O-doped $\mathrm{Bi_2Sr_2CaCu_2O_{8+\delta}}$, $\mathrm{TB1_{loc.\ doped}}$ shows an enhanced superconducting pairing compared to the parent compound model $\mathrm{TB1_{undoped}}$. This model also demonstrates the appearance of the $(\pi,0,0)$ peak in the noninteracting static spin susceptibility. These two features of the doped model prove the suggested important role of local crystal and electronic structure inhomogeneities due to doping for the local superconducting properties of $\mathrm{Bi_2Sr_2CaCu_2O_{8+\delta}}$.

V. CONCLUSIONS

A single-band TB model parametrizing the Cu $3d_{x^2-y^2}$ bands for the high-temperature superconductor $\mathrm{Bi_2Sr_2CaCu_2O_{8+\delta}}$ was derived from DFT electronic-structure calculations. In particular, we analyzed the changes in the TB model parameters induced by the dopant oxygen atom. We found that an accurate quantitative analysis of the dopant-induced changes in the electronic structure of $\mathrm{Bi_2Sr_2CaCu_2O_{8+\delta}}$ requires high-quality TB parametrizations. The required quality of the modeling was achieved by including effective far-neighbor interactions that increased the number of TB parameters in the parent compound model up to 14. Two possible models for the parent compound were proposed and compared, one based on the nearest-neighbors interactions and the second, based on physically justified hybridization paths with an emphasis on intralayer ones. These two parent compound TB models were used for constructing the TB models for the doped supercell. The nontrivial problem of mapping the doped supercell band structure was treated by approximating the doped supercell TB Hamiltonian either by a homogeneous one, with averaged parameters, or by one where only certain selected parameters were adjusted to map the DFT bands. The more promising latter approach gave results consistent with physical intuition when applied to the nearest-neighbors parent compound TB model.

The static spin susceptibility calculated with the doped supercell $\mathrm{TB1_{loc.\ doped}}$ model possesses qualitatively new features, namely, a pronounced peak at the $X=(\pi,0,0)$ point in the folded Brillouin zone, compared to the susceptibility of the parent compound. This change in the susceptibility was shown to lead to a significant enhancement of d-wave pairing in the same $\mathrm{Bi_2Sr_2CaCu_2O_{8+\delta}}$ model. Depending on the value of the interaction parameter U chosen, a modulation of the coupling constant λ of order 30% required to explain the STS phenomenology[2] is easy to obtain. While this is not a strictly local calculation, it is a strong indication that—within weak coupling theory—the local electronic structure change caused by the interstitial O dopant in $\mathrm{Bi_2Sr_2CaCu_2O_{8+\delta}}$ in fact enhances the pairing locally. A full local calculation of the inhomogeneous spin-fluctuation pairing interaction is clearly desirable.

Other extensions of the current calculation would be useful. Since it is known that the three-band model describes the magnetic properties of cuprates better, it would be worthwhile to try to extend the approach presented in this paper by performing a parametrization of the three-band TB Hamiltonian and studying the effects of doping on this model's parameters. In this case, one expects, on the one hand, a growth of the number of model parameters due to new degrees of freedom. On the other hand, the number of effective far-neighbor interactions should decrease as many effects

due to hybridization between Cu and O orbitals are now incorporated in the model itself. One could also consider other *multiband* TB models by taking more Cu and O orbitals, besides the Cu $3d_{x^2-y^2}$, O $2p_x$, and O $2p_y$ orbitals, into account. The multiband models can be very efficiently parametrized within the Slater-Koster formalism;[24] moreover, the formalism allows direct calculation of overlap integrals in the doped compound as a function of relative atomic positions instead of parametrization by fitting. This will be a subject of further investigations.

APPENDIX A: DETAILS OF THE ELECTRONIC-STRUCTURE CALCULATIONS

The Bi$_2$Sr$_2$CaCu$_2$O$_{8+\delta}$ supercell is constructed in the following way. It is rotated with respect to the primitive unit cell by 45° around the z axis and extended along the new x and y axes such that its xy dimensions are $(2\sqrt{2}a \times 2\sqrt{2}a)R45°$, where a is the x dimension of the pure Bi$_2$Sr$_2$CaCu$_2$O$_8$ unit cell. Then only one slab of the two Bi$_2$Sr$_2$CaCu$_2$O$_{8+\delta}$ slabs is considered. In the z direction, the slabs are separated by approximately 15 Å of vacuum in order to exclude any interaction between the marginal Bi atoms of adjacent slabs. The exact atomic positions inside the supercell slab were determined by He *et al.*,[25] who performed structural optimization calculations with the Vienna *ab initio* simulation program (VASP) within the local density approximation.

Calculations for the parent compound were carried out with an energy cutoff for the basis set size given by $R_{MT}K_{max}=5.50$ (R_{MT} is the smallest muffin tin radius and K_{max} is the maximal lattice vector considered). The muffin tin radii for the different atoms in the unit cell were the following: R_{MT}(Bi)=1.88 bohr, R_{MT}(Sr)=2.22 bohr, R_{MT}(Ca)=2.17 bohr, R_{MT}(Cu)=1.82 bohr, and R_{MT}(O) =1.61 bohr. We considered a mesh of 240 k points in the irreducible Brillouin zone (IBZ) corresponding to the space group $I4/mmm$ of the parent compound unit cell. Both $R_{MT}K_{max}$ and the number of k points in the IBZ were tested to be sufficient for rendering an accurate electronic band structure.

The supercell has the symmetry of a centered monoclinic unit cell in the space group Cm which includes as symmetry operations the identity and a mirror plane reflection perpendicular to the atomic layers passing through the interstitial oxygen atom. The atomic displacements caused by the interstitial oxygen are mirror symmetrical about this plane, as illustrated in Fig. 4 for Cu atoms. For the supercell calculations, we used the same $R_{MT}K_{max}$ and R_{MT} values as for the parent compound and 64 k points in the IBZ of the supercell.

APPENDIX B: DETAILS OF THE TIGHT-BINDING MODELS AND APPLICATION TO UNDOPED Bi$_2$Sr$_2$CaCu$_2$O$_8$

The parent compound contains four Cu atoms per unit cell: two Cu atoms per slab. Since the Bi$_2$Sr$_2$CaCu$_2$O$_8$ lattice is base-centered and each eigenvalue in the electronic structure is doubly degenerate due to the presence of two equivalent slabs, there are only two doubly degenerate Cu $3d_{x^2-y^2}$ bands. We therefore construct the TB Hamiltonian by considering only one pair of Cu atoms in one slab

$$H = \sum_{\mathbf{k}} \begin{bmatrix} d_1^\dagger(\mathbf{k}) & d_2^\dagger(\mathbf{k}) \end{bmatrix} \begin{bmatrix} E_{xy}(\mathbf{k}) & E_\perp(\mathbf{k}) \\ E_\perp(-\mathbf{k}) & E_{xy}(\mathbf{k}) \end{bmatrix} \begin{bmatrix} d_1(\mathbf{k}) \\ d_2(\mathbf{k}) \end{bmatrix},$$

(B1)

where $d_i^\dagger(\mathbf{k})$ $[d_i(\mathbf{k})]$ create [annihilate] an electron with a wave vector $\mathbf{k}$ in the Cu $3d_{x^2-y^2}$ orbital of atom $i=1,2$ (Cu atoms 1 and 2 belong to different CuO$_2$ layers). The energy dispersion $E_{xy}(\mathbf{k})$ is due to interactions between Cu atoms within a layer and $E_\perp(\mathbf{k})$ is due to interlayer electron hoppings; both dispersions are given by

$$E_{xy,\perp}(\mathbf{k}) = \sum_{\mathbf{l}} \exp(i\mathbf{k}\cdot\mathbf{l})t_{\mathbf{l}},$$

where $t_{\mathbf{l}}$ is the hopping integral between Cu atoms that are connected by a vector $\mathbf{l}$. This vector is denoted as $\mathbf{l} =(n,m,z)$ and corresponds to a vector (na,ma,zc) in absolute coordinates where a and c are the unit-cell parameters, n,m denote integers and $z=0.099$, is the distance between two CuO$_2$ layers in units of c.

By optimizing the values of the hopping integrals $t_{\mathbf{l}}$, the eigenvalues of the Hamiltonian Eq. (B1) can be adjusted to describe the Cu $3d_{x^2-y^2}$ bands of the parent compound. In order to obtain a description that satisfies our accuracy requirements, we had to include into the model effective hopping integrals between 12 Cu nearest neighbors as listed in Table I. We denote this tight-binding results TB1$_{undoped}$.

The in-plane nearest-neighbor hopping integral $t_{100}=$ -0.5196 eV and second nearest-neighbor hopping integral $t_{110}=0.1115$ eV are in agreement with the results of previous DFT calculations[12] and with the analysis of photoemission measurements of the Bi$_2$Sr$_2$CaCu$_2$O$_8$ electronic structure.[26] In Fig. 2(a), the energy spectrum of the TB Hamiltonian is compared with the DFT bands. The agreement is overall good, except for some small deviations around the Γ point. This region is particularly difficult to reproduce since here the shape of the Cu $3d_{x^2-y^2}$ bands is strongly influenced by the hybridizations between the Cu $3d_{x^2-y^2}$ orbital and other energetically close Cu d and O p orbitals.

APPENDIX C: DETAILS OF THE TB MODEL FOR THE O-DOPED SUPERCELL

Here, we present the TB model for the O-doped supercell, based upon the TB1$_{undoped}$ model for the undoped single cell,

whose parameters we use as initial. As adjustable parameters, we choose three hopping integrals of the t_{100} type, two of the t_{110} type, and three of the t_{200} type that connect the Cu atoms experiencing the largest displacement due to the interstitial oxygen and its neighbors (the hopping integrals of the t_{100}, t_{110}, and t_{200} types are represented by, respectively, solid, dashed and dash-dotted lines in Fig. 4). We also allow for different on-site energies μ for the $3d_{x^2-y^2}$ orbitals of the 8 Cu atoms in the CuO_2 layer closest to the dopant. Making use of the crystal symmetry, the number of μ parameters is reduced to six. We then assign a unique μ value to the on-site energies of the other eight Cu atoms since we expect that they are less affected by the dopant. These seven on-site energies together with the eight hopping integrals are varied during the Hamiltonian optimization. The optimized values of the hopping integrals are given in Fig. 4 in eV and the on-site energies are listed in the Figure caption. We denote this model $TB1_{loc.\ doped}$. We observe the largest on-site energy variation for the most displaced Cu (marked with an arrow in Fig. 4) while Cu further away from the dopant are hardly affected. The variations in the hopping integrals are

also consistent. For example, t_{100} increases when the two Cu atoms get closer and slightly decreases when they are pushed apart by the interstitial oxygen. The decrease is even stronger when the Cu atoms shift with respect to each other parallel to the mirror plane, what appreciably reduces the orbital overlap.

We also considered the same 15 parameters (7 μ's and 8 t's) to map the DFT Cu $3d_{x^2-y^2}$ bands with a supercell TB Hamiltonian based upon the $TB2_{undoped}$ for the parent compound, Table II. While a mapping to the doped bands is almost as good as the one given by the previous model, the resulting model parameters assumed seemingly chaotic values not consistent with their expected behavior. One faces similar inconsistencies also when other trial sets of adjustable parameters are used. The failure of the $TB2_{undoped}$ (Table II) in describing the dopant-induced changes in the band structure of $Bi_2Sr_2CaCu_2O_{8+\delta}$ indicates that the results provided by the approach based on optimizing certain selected model parameters depend very strongly on the choice of effective far neighbor interactions that are not optimized.

---

[1] K. McElroy, J. Lee, J. A. Slezak, D.-H. Lee, H. Eisaki, S. Uchida, and J. C. Davis, Science **309**, 1048 (2005).

[2] T. S. Nunner, B. M. Andersen, A. Melikyan, and P. J. Hirschfeld, Phys. Rev. Lett. **95**, 177003 (2005).

[3] M. M. Maśka, Ź. Śledź, K. Czajka, and M. Mierzejewski, Phys. Rev. Lett. **99**, 147006 (2007).

[4] S. Johnston, F. Vernay, and T. P. Devereaux, EPL **86**, 37007 (2009).

[5] K. Foyevtsova, R. Valentí, and P. J. Hirschfeld, Phys. Rev. B **79**, 144424 (2009).

[6] T. A. Maier, D. Poilblanc, and D. J. Scalapino, Phys. Rev. Lett. **100**, 237001 (2008).

[7] L. de' Medici, X. Wang, M. Capone, and A. J. Millis, Phys. Rev. B **80**, 054501 (2009).

[8] J. K. Liang, S. S. Xie, G. C. Che, J. Q. Huang, Y. L. Zhang, and Z. X. Zhao, Mod. Phys. Lett. B **2**, 483 (1988).

[9] Y. He, S. Graser, P. J. Hirschfeld, and H.-P. Cheng, Phys. Rev. B **77**, 220507(R) (2008).

[10] P. Blaha, K. Schwarz, G. K. H. Madsen, D. Kvasnicka, and J. Luitz, in WIEN2K, An Augmented Plane Wave Plus Local Orbitals Program for Calculating Crystal Properties, edited by Karlheinz Schwarz (Technical Universität, Wien, Austria, 2001).

[11] J. P. Perdew, K. Burke, and M. Ernzerhof, Phys. Rev. Lett. **77**, 3865 (1996).

[12] See, for instance, R. S. Markiewicz, S. Sahrakorpi, M. Lindroos, H. Lin, and A. Bansil, Phys. Rev. B **72**, 054519 (2005).

[13] See, for instance, H. C. Kandpal, I. Opahle, Y.-Z. Zhang, H. O. Jeschke, and R. Valentí, Phys. Rev. Lett. **103**, 067004 (2009).

[14] S. Graser, T. A. Maier, P. J. Hirschfeld, and D. J. Scalapino, New J. Phys. **11**, 025016 (2009).

[15] O. K. Andersen, O. Jepsen, A. I. Liechtenstein, and I. I. Mazin, Phys. Rev. B **49**, 4145 (1994).

[16] P. W. Anderson, Science **235**, 1196 (1987).

[17] A. E. Ruckenstein, P. J. Hirschfeld, and J. Appel, Phys. Rev. B **36**, 857 (1987).

[18] G. Baskaran, Z. Zou, and P. W. Anderson, Solid State Commun. **63**, 973 (1987).

[19] E. Pavarini, I. Dasgupta, T. Saha-Dasgupta, O. Jepsen, and O. K. Andersen, Phys. Rev. Lett. **87**, 047003 (2001).

[20] G. D. Mahan, Many-Particle Physics (Springer, Netherlands, 2000).

[21] N. E. Bickers, D. J. Scalapino, and S. R. White, Phys. Rev. Lett. **62**, 961 (1989).

[22] N. Bulut and D. J. Scalapino, J. Phys. Chem. Solids **54**, 1109 (1993).

[23] W. D. Wise, M. C. Boyer, K. Chatterjee, T. Kondo, T. Takeuchi, H. Ikuta, Y. Wang, and E. W. Hudson, Nat. Phys. **4**, 696 (2008).

[24] J. Slater and G. Koster, Phys. Rev. **94**, 1498 (1954).

[25] Y. He, T. S. Nunner, P. J. Hirschfeld, and H.-P. Cheng, Phys. Rev. Lett. **96**, 197002 (2006).

[26] R. J. Radtke and M. R. Norman, Phys. Rev. B **50**, 9554 (1994).